PHYSICAL REVIEW C VOLUME 22, NUMBER 3 SEPTEMBER 1980

Current densities in the projected Hartree-Fock approach. II. Transverse form factors

E. Moya de Guerra
Center for Theoretical Physics, Laboratory for Nuclear Science and Department of Physics, Massachusetts Institute of Technology, Cambridge, Massachusetts 02139

S. Kowalski
Bates Accelerator Center, Laboratory for Nuclear Science and Department of Physics, Massachusetts Institute of Technology, Cambridge, Massachusetts 02139

(Received 5 November 1979)

Collective and single-particle contributions to transverse form factors of rotational nuclei have been computed in the projected Hartree-Fock approach using the density matrix expansion effective Hamiltonian. Results on several odd-A rare earth nuclei (^{181}Ta, ^{165}Ho, ^{159}Tb) are presented and compared to the available experimental data. Theoretical predictions for transverse electric form factors of ^{166}Er are also presented. A comparison is made of the resulting form factors as $q \to 0$ with those extracted from measured transition probabilities $B(E(M)\lambda; I_i \to I_f)$.

[NUCLEAR STRUCTURE ^{159}Tb, ^{165}Ho, ^{166}Er, ^{181}Ta; calculated elastic and inelastic transverse form factors. Angular momentum projected Hartree-Fock approximation.]

I. INTRODUCTION

Electron scattering experiments on ^{181}Ta at 180° are now being performed[1] at the Bates Linear Accelerator Center and experiments on other rare earth rotational nuclei are planned for the near future. It is well known[2] that such experiments measure transverse form factors and in turn provide information on nuclear currents.

The transverse form factors for elastic and inelastic scattering within a given rotational band can be written in terms of intrinsic current density multipoles[3] which contain the information on the intrinsic structure of the band. The limited experimental information presently available[1] does not make it possible to extract detailed information about the rotational current. From a theoretical point of view the projected Hartree-Fock approach[3,4] (PHF) provides a plausible first step for investigating these properties for the first few states in the ground-state rotational band. In this case, the intrinsic structure is not expected to be drastically modified by the rotation, as confirmed by experimental information[5] on charge distributions of rare earth nuclei.

Although the projection after variation method does not in general lead to the right inertial parameters[6] and its description of rotational properties is questionable, it has been shown,[7] however, that it leads to collective gyromagnetic ratios in good agreement with experimental ones. One may therefore expect that it would give a reasonable description of the collective current distribution.

To first order in $1/\langle J_\perp^2 \rangle$ the PHF approach leads to a decomposition of the transverse form factors in terms of single particle and collective form factors.[4] This decomposition is analogous to the one obtained[3] by keeping first order terms in $I_\pm$ in the general transformation[8] of tensor operators into the intrinsic coordinate system. This is briefly discussed in Sec. II where a summary of the theory is presented. The calculations were done in plane wave Born approximation (PWBA), details given in Appendix A, with the results presented in Sec. III. A detailed discussion of the results on ^{166}Er and ^{181}Ta is given in Secs. IIIA and IIIB, respectively. The calculated transverse form factors for ^{159}Tb, ^{165}Ho, and ^{166}Er and ^{181}Ta are presented in Sec. IIIC where a comparison is made with available experimental data from electron scattering as well as from γ transitions (extrapolated to $q = 10^{-3}$ fm^{-1}).

II. SUMMARY OF THEORY

Following the notation of DeForest and Walecka[9] we write the differential cross section at 180° for elastic and inelastic scattering within the ground-state rotational band (K) as

$$\left.\frac{d\sigma(E,\theta=\pi)}{d\Omega}\right|_{I_iK\to I_fK} = \frac{Z^2\alpha^2}{4E^2}(1+2E/M_{\text{targ}})^{-1}\cdot F_T^2(q)\,|_{I_iK\to I_fK}\,, \tag{2.1}$$

where the transverse form factor squared is given by

 © 1980 The American Physical Society

$$F_T^2(q)\,|_{I_iK\to I_fK} = \sum_{\lambda=\text{even}>0} [F^{E\lambda}_{I_f}(q)]^2 + \sum_{\lambda=\text{odd}} [F^{M\lambda}_{I_f}(q)]^2 \qquad (2.2)$$

with

$$\frac{Z}{\sqrt{4\pi}} F^{E\lambda}_{I_f}(q) = \frac{\langle I_fK \| T^{E\lambda}(q) \| I_iK\rangle}{(2I_i+1)^{1/2}}\,,$$

$$\frac{Z}{\sqrt{4\pi}} F^{M\lambda}_{I_f}(q) = \frac{\langle I_fK \| T^{M\lambda}(q) \| I_iK\rangle}{(2I_i+1)^{1/2}}\,. \qquad (2.3)$$

The one body transverse electric and magnetic operators are defined as in Ref. 9 with a factor i^λ so that the relevant reduced matrix elements in (2.3) are real. The latter can be written as linear combinations of intrinsic matrix elements weighted by different angular momentum dependent coefficients. As in the case of $M1$ and $E2$ γ transitions, a "model independent"[8] decomposition of the form factors can be made into intrinsic ones based on general symmetry principles. It can also be shown[3] that, to first order in $I_\pm$,[8] such an analysis leads to the results summarized below for the cases of interest here, $I_f \geq I_i = K$.

Odd-A nuclei

$$F^{M\lambda}_{I_f}(q) = \langle KK\lambda 0 \,|\, I_fK\rangle \left[F^{M\lambda}_K(q) + \frac{\langle K-K\lambda 2K \,|\, I_fK\rangle}{\langle KK\lambda 0 \,|\, I_fK\rangle} \times F^{M\lambda}_{2K}(q)\right] + \langle KK\lambda 0 \,|\, I_fK\rangle \frac{[\lambda(\lambda+1)+K(K+1)-I_f(I_f+1)]}{[2\lambda(\lambda+1)]^{1/2}} \times F^{M\lambda}_R(q)\,, \qquad (2.4)$$

$$F^{E\lambda}_{I_f}(q) = \langle K-K\lambda 2K \,|\, I_fK\rangle F^{E\lambda}_{2K}(q) + \langle KK\lambda 0 \,|\, I_fK\rangle \times [I_f(I_f+1)-K(K+1)]F^{E\lambda}_R(q)\,. \qquad (2.5)$$

Even-even nuclei ($K=0$)

$$F_T(q)\,|_{00\to I_f0} = \delta_{I_f,\lambda} F^{E\lambda}_{I_f}(q) = I_f(I_f+1)F^{E\lambda}_R(q)\delta_{I_f,\lambda}\,. \qquad (2.6)$$

Equations (2.4)–(2.6) are model independent in the sense that they do not depend on the particular model used to describe the rotational band—provided that a first order expansion in angular momentum is valid—nor do they depend on the particular approximation to the operators $T^{E(M)\lambda}$ (whether they are the usual one body operators or include terms coming from exchange currents). These characteristics will only be reflected in the predictions of different models to the intrinsic multipoles.[3] The intrinsic form factors $F^{M\lambda}_K(q)$, $F^{M(E)\lambda}_{2K}(q)$, and $F^{M(E)\lambda}_R(q)$ are to this order independent of initial and final spins and depend only on the intrinsic structure of the (ground state) band. They could, at least in principle, be determined by an analysis of precise experimental data on transverse form factors. This renders the situation analogous to the analyses of γ transitions in terms of the familiar gyromagnetic ratios and quadrupole moments.[8] To establish this analogy in a more explicit way we notice that in the long-wavelength limit the intrinsic form factors defined above are given by

$$F^{M1}_K(q) \underset{q\to 0}{\longrightarrow} \frac{1}{Z}\left(-\frac{\hbar q}{2Mc}\right)\left(\tfrac{2}{3}\right)^{1/2} K g_K\,, \qquad (2.7)$$

$$F^{M1}_R(q) \underset{q\to 0}{\longrightarrow} \frac{1}{Z}\left(-\frac{\hbar q}{2Mc}\right)\left(\tfrac{2}{3}\right)^{1/2} g_R\,, \qquad (2.8)$$

$$F^{M1}_{2K}(q) \underset{q\to 0}{\longrightarrow} \frac{1}{Z}\left(-\frac{\hbar q}{2Mc}\right)\left(\tfrac{2}{3}\right)^{1/2}\left(-\frac{1}{\sqrt{2}}\right)(g_K - g_R)b\,, \quad \text{for } K=\tfrac{1}{2}\,, \qquad (2.9)$$

$$F^{E\lambda}_R(q) \underset{q\to 0}{\longrightarrow} \frac{1}{Z}\frac{(-i^\lambda)q^{\lambda-1}}{(2c\vartheta/\hbar)(2\lambda+1)!!} \times \left(\frac{\lambda+1}{\lambda}\right)^{1/2}\left(\frac{2\lambda+1}{4}\right)^{1/2} Q^p_\lambda\,, \qquad (2.10)$$

where g_K, g_R, and b (the magnetic decoupling parameter) are defined in Ref. 8. The last relation (2.10) follows from the continuity equation.[9] Consistent with the expressions (2.5) and (2.6) only the lowest order terms in angular momentum have been kept for the longitudinal form factor and for the energy difference. ϑ is the moment of inertia (in units of $\hbar^2\text{MeV}^{-1}$) and the Q_λ multipoles are, as defined in Refs. 8 and 10,

$$Q^p_\lambda = \left(\frac{16\pi}{2\lambda+1}\right)^{1/2} \int d\vec{R}\, R^\lambda Y^0_\lambda(\hat{R})\rho_p(\vec{R})\,. \qquad (2.11)$$

Finally $F^{E\lambda}_{2K}$ is proportional, in the long-wavelength limit, to the signature dependent term in $B(E\lambda)$ (Ref. 8) (and to the decoupling parameter a in bands with $K=\frac{1}{2}$). This relation—as well as those corresponding to higher magnetic multipoles—is not so useful and has been omitted here.

The relations (2.7)–(2.10) are interesting for two reasons.

(1) They serve to estimate the transverse form factors at low q ($q<1/R$) from experimentally known gyromagnetic ratios and quadrupole moments.

(2) For theoretical calculations of the intrinsic form factors within a model, they serve to check the validity of the model as well as the internal consistency of the model calculations. We will come back to this point at the end of Sec. III where our PHF results are discussed.

In the PHF approach the intrinsic form factors defined above are given[3,4] by

$$F_K^{M\lambda}(q)=\frac{\sqrt{4\pi}}{Z}\langle\phi_K|T_0^{M\lambda}(q)|\phi_K\rangle, \tag{2.12}$$

$$F_{2K}^{M\lambda}(q)=\frac{\sqrt{4\pi}}{Z}\langle\phi_K|T_{2K}^{M\lambda}(q)|\phi_{\bar{K}}\rangle, \tag{2.13}$$

$$F_R^{M\lambda}(q)=\frac{\sqrt{4\pi}}{Z}\frac{(-\sqrt{2})}{\langle J_\perp^2\rangle}\,\mathrm{Re}\langle\phi_K|T_1^{M\lambda}(q)J_-|\phi_K\rangle, \tag{2.14}$$

$$F_{2K}^{E\lambda}(q)=\frac{\sqrt{4\pi}}{Z}\langle\phi_K|T_{2K}^{E\lambda}(q)|\phi_{\bar{K}}\rangle, \tag{2.15}$$

$$F_R^{E\lambda}(q)=\frac{\sqrt{4\pi}}{Z}\frac{[\lambda(\lambda+1)]^{-1/2}}{\langle J_\perp^2\rangle}\,\mathrm{Re}\langle\phi_K|T_1^{E\lambda}(q)J_-|\phi_K\rangle. \tag{2.16}$$

$F_K^{M\lambda}(q)$ also contains a term proportional to $1/\langle J_\perp^2\rangle$. The contribution of this term to g_K was calculated in Ref. 7 and shown to be negligible; we have therefore omitted it in the present calculations. The notation used here follows that of Refs. 4 and 7. $\vec{J}=\sum_i \vec{j}_i$ is the total angular momentum operator divided by $\hbar$. In particular, these calculations have been done with the same Hartree-Fock wave functions (ϕ_K) as used in Ref. 7. These wave functions have the property that the even-even core is time reversal invariant and only the odd nucleon contributes to $F_K^{M\lambda}$ and $F_{2K}^{M(E)\lambda}$. On the other hand, $F_R^{M(E)\lambda}$ receives equal contributions from time reversed orbitals. We refer to the first term in Eqs. (2.4) and (2.5) as the single particle contribution and to the second term as the collective contribution.

For even-even nuclei the matrix elements $\langle T_1^{\sigma\lambda}J_-\rangle$ (with $\sigma=E,M$) are given by

$$\begin{aligned}\mathrm{Re}\langle T_1^{\sigma\lambda}J_-\rangle&=\sum_{A,B}\theta_{AB}(\langle A|T_1^{\sigma\lambda}|B\rangle\langle A|j_+|B\rangle\\&\quad+\tfrac{1}{2}\langle A|T_1^{\sigma\lambda}|\bar{B}\rangle\langle A|j_+|\bar{B}\rangle),\end{aligned} \tag{2.17}$$

$$\begin{aligned}&=\sum_A n_A\langle A|T_1^{\sigma\lambda}j_-+(-1)^\lambda T_{-1}^{\sigma\lambda}j_+|A\rangle\\&\quad-\sum_{A,B}\theta'_{AB}(2\langle A|T_1^{\sigma\lambda}|B\rangle\langle A|j_+|B\rangle\\&\qquad+\langle A|T_1^{\sigma\lambda}|\bar{B}\rangle\langle A|j_+|\bar{B}\rangle).\end{aligned} \tag{2.17'}$$

For odd-A nuclei, corrections similar to those in Ref. 7 must be applied to Eqs. (2.17) and (2.17′) [with s_+, s_- replaced by $T_1^{\sigma\lambda}$, $(-1)^\lambda T_{-1}^{\sigma\lambda}$, respectively; also see Appendix A]. In the previous equations A and B denote single particle HF states (with $m>0$), and θ'_{AB} and θ_{AB}, as shown below, depend on the occupation numbers n_A and n_B:

$$\theta'_{AB}=n_An_B+[n_A(1-n_A)n_B(1-n_B)]^{1/2}, \tag{2.18}$$

$$\theta_{AB}=n_A+n_B-2\theta'_{AB}. \tag{2.19}$$

The collective form factors for ^{166}Er and ^{181}Ta were computed using both expressions (2.17) and (2.17′) (or their equivalents for odd-A nuclei). As in the case of collective gyromagnetic ratios[7] the results were almost identical. The calculations on ^{165}Ho and ^{159}Tb were performed using Eq. (2.17), since this saved a considerable amount of computation time. The explicit expressions used in the computer codes as well as other details of the calculation can be found in Appendix A. They apply to calculations with and without pairing. In the case of no pairing, $\theta_{AB}=1$ for A occupied and B unoccupied (or vice versa), and zero otherwise.

III. DISCUSSION OF RESULTS AND COMPARISON WITH EXPERIMENT

An interesting aspect of electron scattering at 180° on rotational nuclei is that one can extract information on the distribution of the collective rotational current density.

Experiments on even-even nuclei would provide this information in a direct way. Inelastic scattering experiments[12] have recently begun on ^{166}Er to measure transverse electric form factors [see Eq. (2.6)]. Transverse magnetic form factors could in principle be measured directly by elastic scattering on excited states. Therefore the only experimentally available information on them will be from static moments.

In the case of odd-A nuclei a model is needed to separate single particle contributions from collective ones. Even in the case that Eqs. (2.4) and (2.5) represent a good approximation, it is clear that very precise data (on scattering to several levels) are required to disentangle the different contributions to the various electric and magnetic multipoles. However, it is important to have an estimate of the relative magnitude of single particle and collective form factors in a model that has been previously tested for static moments and longitudinal form factors. The PHF approach, to first order in $1/\langle J_\perp^2\rangle$,[7,10,13] is such a model.

With this objective we present the details of the PHF results for ^{166}Er and ^{181}Ta in Secs. III A and III B, respectively. In order to facilitate the comparison with other theoretical calculations, corrections due to nucleon finite size and center of mass effects are not included. These effects have only been included in the total transverse form factors presented in Sec. III C in order to compare with experimental data. For purposes of clarity, form factors maxima below $\sim 2.5\times10^{-10}$ are not shown in the figures.

An important question in assessing the validity of these results is that of numerical accuracy and convergence of the PHF solutions. The numerical procedure that was used is similar to that developed by Negele and Rinker[10] in the calculation of

transition charge densities $\rho_l(r)$ for deformed nuclei. In their work it was shown that the convergence of $\rho_l(r)$ degrades with increasing l. To minimize these effects, a large oscillator basis $N_0 = 12$ was used and the number of HF iterations was increased beyond the point where the hexadecapole moment ($Q4$) converged to within a few percent of its projected asymptotic value. Approximately 100 iterations were required. Our results for the transverse form factors showed no appreciable (<5%) change as we further doubled the number of HF iterations.

A. Results on ^{166}Er

The transverse form factors for inelastic scattering on ^{166}Er are plotted in Fig. 1 for $I_f = 2, 4, 6$ [see Eq. (2.6)]. The solid curve shows the results corresponding to occupation numbers 0 or 1 (no pairing) and the dashed curves are the results with pairing. The main effect of pairing is to increase the maxima below $q \sim 1$ fm^{-1} and to decrease those at higher momentum transfer. The first can be associated with the fact that pairing brings more contributions from outer shells into $F_R^{E\lambda}$. It is interesting, however, to note that the increase

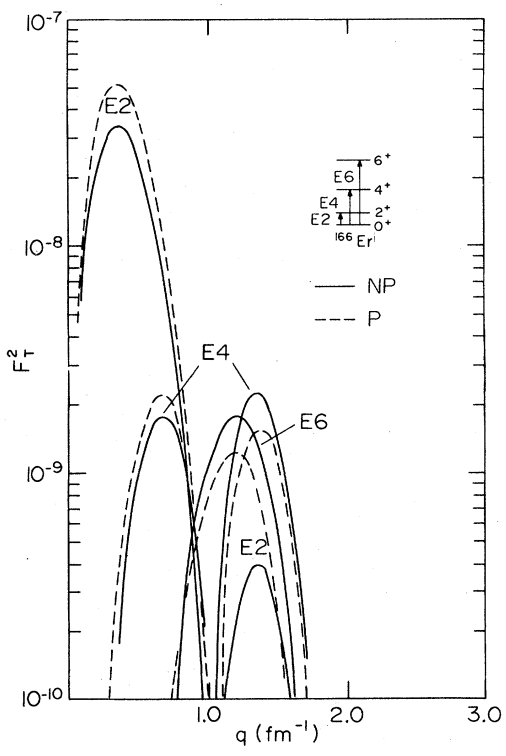

FIG. 1. Calculated transverse form factors for ^{166}Er. Results corresponding to pairing (P) and no pairing (NP) are represented by dashed and full lines, respectively.

in the first peak of the $E2$ is approximately equal to the ratio $(\langle J_\perp^2\rangle^{NP}/\langle J_\perp^2\rangle^{P})^2 = 1.6$ [see Eq. (2.16) and Ref. 7]. The decrease of the $E6$ and second peaks of $E2$ and $E4$ is mainly due to a decrease in the magnetization contribution [terms in μ_α in Eq. (A7)]. The magnetization contribution—which is negligible at low q—plays an important role in the formation of the peaks at $q > 1$ fm^{-1} where it is 3 to 4 times larger than the convection contribution.

B. Results on ^{181}Ta

For odd-A nuclei the transverse electric and magnetic form factors separate into single particle and collective contributions [see Eqs. (2.4), (2.5), and (2.12)–(2.16)],

$$F_{I_f}^{\sigma\lambda}(q) = (F_{I_f}^{\sigma\lambda})_{\text{s.p.}} + (F_{I_f}^{\sigma\lambda})_{\text{col}}, \quad \sigma = E, M \tag{3.1}$$

with

$$(F_{I_f}^{M\lambda})_{\text{s.p.}} = \langle KK\lambda 0 \,|\, I_f K\rangle F_K^{M\lambda}(q) + \langle K - K\lambda 2K \,|\, I_f K\rangle F_{2K}^{M\lambda}(q), \tag{3.2}$$

$$(F_{I_f}^{M\lambda})_{\text{col}} = \langle KK\lambda 0 \,|\, I_f K\rangle \frac{[\lambda(\lambda+1) + K(K+1) - I_f(I_f+1)]}{[2\lambda(\lambda+1)]^{1/2}} \times F_R^{M\lambda}(q), \tag{3.3}$$

$$(F_{I_f}^{E\lambda})_{\text{s.p.}} = \langle K - K\lambda 2K \,|\, I_f K\rangle F_{2K}^{E\lambda}(q), \tag{3.4}$$

$$(F_{I_f}^{E\lambda})_{\text{col}} = \langle KK\lambda 0 \,|\, I_f K\rangle [I_f(I_f+1) - K(K+1)] F_R^{E\lambda}(q). \tag{3.5}$$

In order to show the relative intensity of single particle and collective contributions for elastic and inelastic scattering on ^{181}Ta, $(F_{I_f}^{\sigma\lambda})_{\text{s.p.}}{}^2$ and $(F_{I_f}^{\sigma\lambda})_{\text{col}}{}^2$ are plotted separately in Figs. 2–6 and 7–9, respectively. The relative sign of $(F_{I_f}^{\sigma\lambda})_{\text{col}}$ to $(F_{I_f}^{\sigma\lambda})_{\text{s.p.}}$ for identical multipoles is also indicated in Figs. 7–9.

In Figs. 2 and 3 the HF results for single particle form factors are compared to the results with Nilsson wave functions in a spherical basis.[4,8] The difference between them is due to the fact that the HF single particle wave function contains many small admixtures of higher N shells. As a consequence, the strength of the $M1$, $M7$ ($E8$) peaks is slightly reduced (enhanced) and the peak of the $M7$ is moved to lower momentum transfer. As pointed out in Ref. 4, the suppression of the intermediate multipoles ($M3$, $M5$) is due to angular momentum coupling in the intrinsic system. The reduction of the single particle form factors in rotational nuclei (as compared to spherical ones)[4] can be understood from the fact that the total strength is shared by elastic and inelastic form factors [see Eq. (3.2) and Figs. 2–6].

The calculations were done (see Appendix A) using nucleon charges (e_i) and magnetic moments

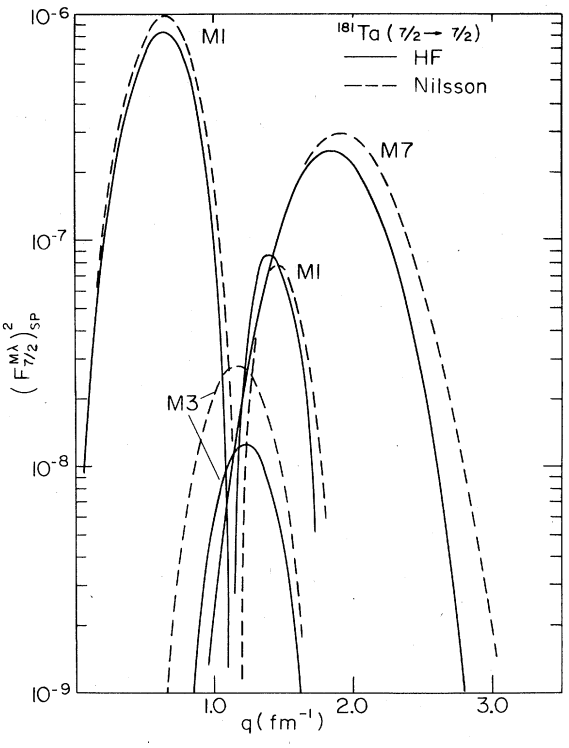

FIG. 2. Single particle contributions (squared) to transverse form factors (as defined in text) for elastic scattering on ^{181}Ta. The various multipole distributions corresponding to HF and Nilsson wave functions are represented, respectively, by full and dashed curves. The Nilsson results correspond to an oscillator range parameter $b = 2.2$ fm.

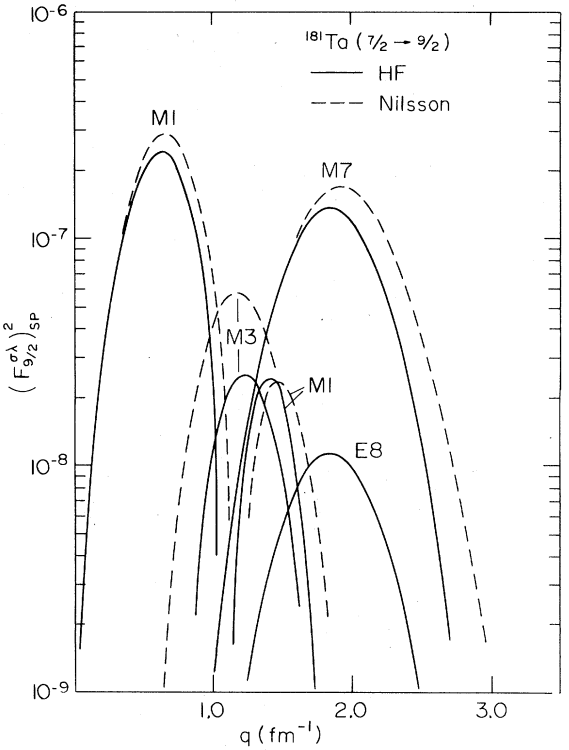

FIG. 3. Same as Fig. 2 for the transition $\frac{7}{2} \rightarrow \frac{9}{2}$ in the ground-state band.

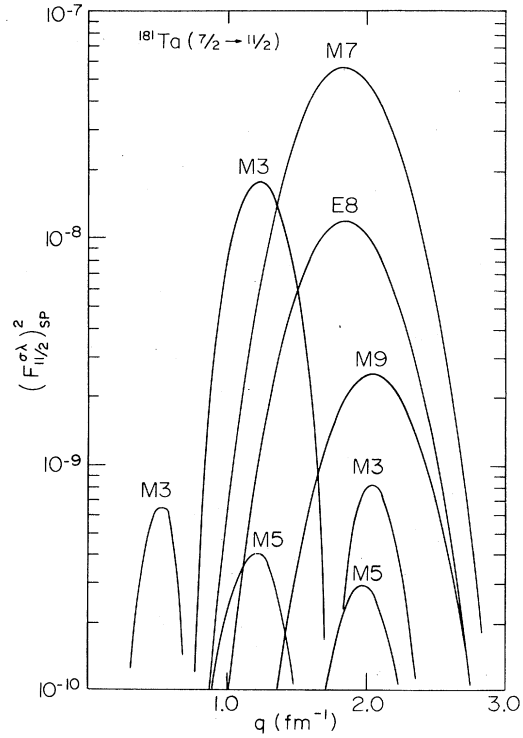

FIG. 4. Same as Fig. 2 for the transition $\frac{7}{2} \rightarrow \frac{11}{2}$ in the ground-state band. Only results corresponding to HF wave functions are shown.

(μ_i) corresponding to free nucleons. As discussed in Ref. 7 the lack of spin polarization in the HF wave functions leads to g_K values significantly different from experimental ones. This effect is usually[8] accounted for by introducing effective values for the odd nucleon magnetic moment. A calculation of the single particle $M1$ form factor was performed using $g_s^{\text{eff}} = 0.48 g_s^{\text{free}}$.[7] It was found that the main effect was to lower the first peak of the $M1$ from $8.4(10^{-7})$ to $7.8(10^{-7})$ and to displace it slightly to lower q (from $q \sim 0.62$ fm^{-1} to $q \sim 0.53$ fm^{-1}). The small size of this effect is due to the fact that at the peak of the $M1$ the convection part is approximately 4 times larger than the magnetization part and both add coherently. This is in contrast to what happens as $q \rightarrow 0$. As an alternative, effective g_l values can be used. To fit the experimental g_K value[7] one can also choose $g_l^{\text{eff}} = g_l^{\text{free}} + \delta g_l$ with $\delta g_l = 0.36$ and $g_s = g_s^{\text{free}}$. This leads to an enhancement in the $M1$ form factor at $q \sim 0.62$ fm^{-1} by a factor of 1.7. However the q dependence of spin polarization effects—as well as those due to

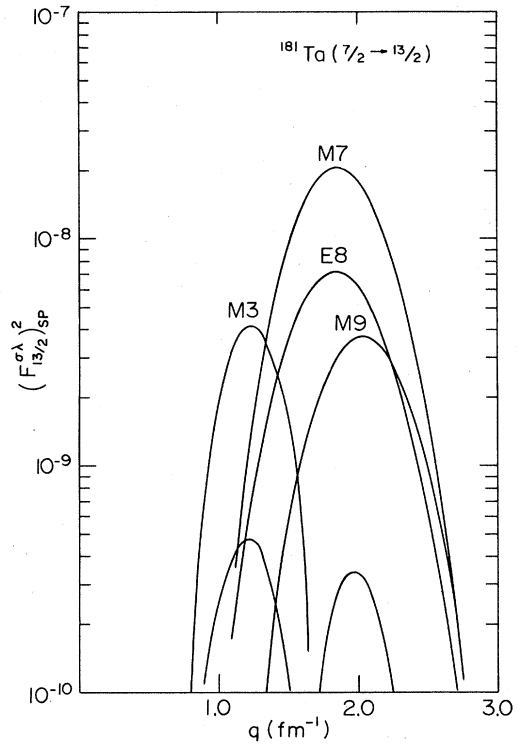

FIG. 5. Same as Fig. 4 for the transition $\frac{7}{2} \rightarrow \frac{13}{2}$.

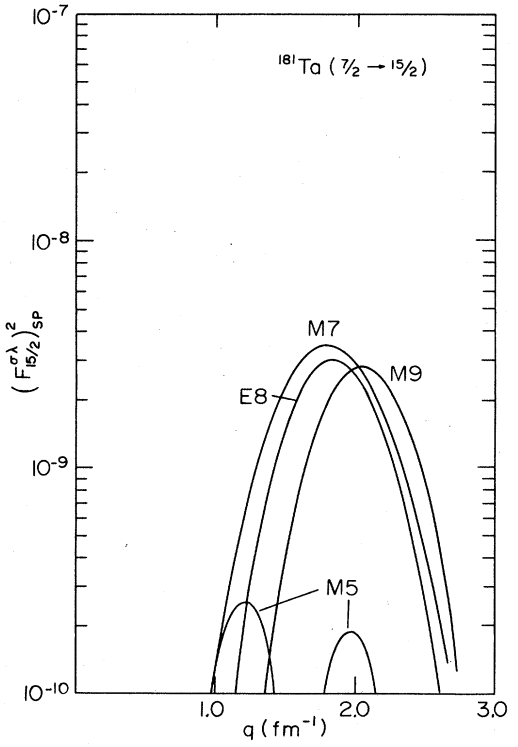

FIG. 6. Same as Fig. 4 for the transition $\frac{7}{2} \rightarrow \frac{15}{2}$.

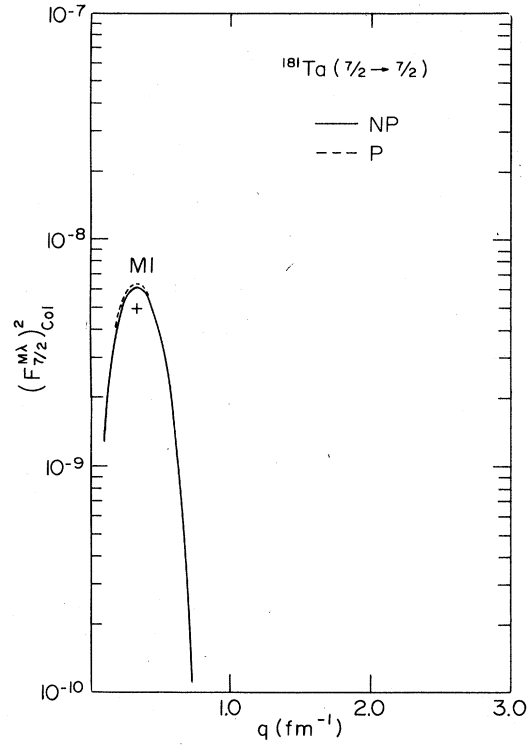

FIG. 7. Collective contributions (squared) to transverse magnetic multipoles (see text) for elastic scattering on ^{181}Ta. Results corresponding to pairing (P) and no pairing (NP) are represented by dashed and full lines, respectively. The multipole distributions with $\lambda \geq 3$ are less than 10^{-10}. The sign in the first peak of the $M1$ refers to the relative sign of collective and single particle amplitudes in the q region from 0 to ~ 0.75 fm^{-1}.

exchange currents[14]—can be important and may not be well simulated by introducing effective g_l, g_s values. We leave this question open for further investigation.

The results for collective form factors are shown in Figs. 7–9. The peaks of the form factors with $\lambda \geq 3$, are less than 2.5×10^{-10} in all transitions and have not been plotted. As can be seen the results for the form factors corresponding to pairing (dashed curves) and no pairing (full curves) are similar. For elastic scattering the collective and single particle contributions add coherently from $q = 0$ to $q \sim 0.75$ [this is indicated by a (+) sign in Fig. 7]. The first is about 24 times smaller than the second at $q \sim 0.62$ and its main effect is to increase the first peak of the $M1$ from 8.4×10^{-7} to 9.1×10^{-7} (see Fig. 10). On the contrary, for inelastic scattering ($I_f = \frac{9}{2}$) the sign of single particle and collective contributions is opposite [indicated by (–) in Fig. 8] in the above mentioned q region; furthermore the collective contribution is only 7 times smaller than the single particle at $q \sim 0.62$.

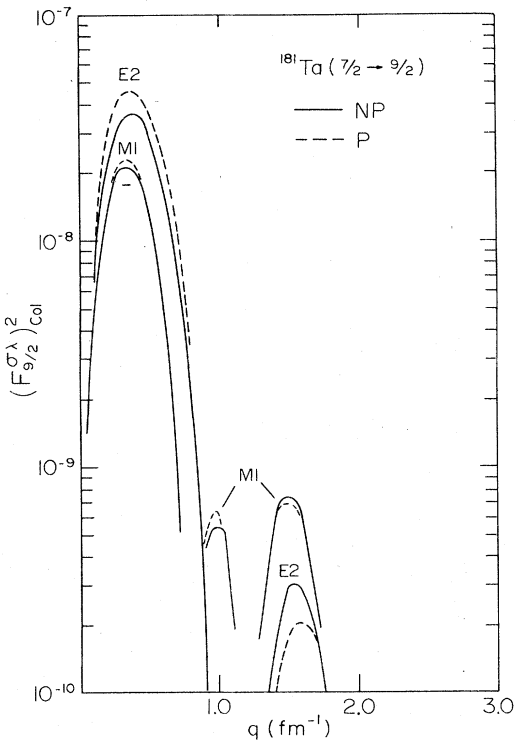

FIG. 8. Collective contributions (squared) to transverse electric and magnetic multipoles for the transition $\frac{7}{2} \rightarrow \frac{9}{2}$ in the ground-state band in ^{181}Ta. Results corresponding to pairing (P) and no pairing (NP) are represented by dashed and full lines, respectively. The multipole distributions and with $\lambda \geq 3$ are less than 10^{-10}. The sign in the first peak of the $M1$ refers to the relative sign of collective and single particle amplitudes in the q region from 0 to ~0.75 fm^{-1}.

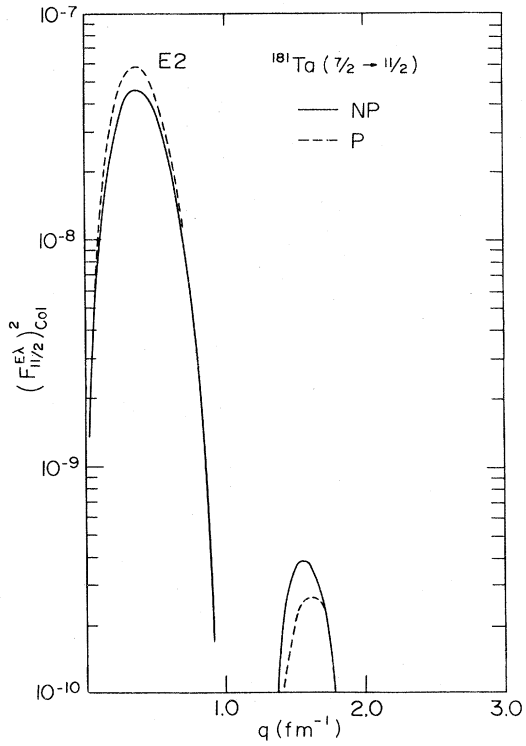

FIG. 9. Collective contributions (squared) to transverse electric multipoles for the transition $\frac{7}{2} \rightarrow \frac{11}{2}$ in the ground-state band of ^{181}Ta. Both peaks correspond to the $\lambda = 2$ multipole (see text).

This results in a shift of the first peak of the $M1$ to a larger q ($q \sim 0.7$ fm^{-1}) and reduces its amplitude by 16%. The reason for this difference between $M1$ elastic and inelastic form factors is that $F_K^{M1}(q)$ and $F_R^{M1}(q)$ combine differently [see Eq. (2.4)].

A more significant collective effect is the $E2$ contribution to inelastic scattering in the transition $\frac{7}{2} \rightarrow \frac{11}{2}$ (see Figs. 4 and 9), where the single particle form factor at low q is negligible. The effect of pairing in this case is analogous to that in ^{166}Er but somewhat smaller due in part to the odd nucleon and in part to the smaller gap parameters.[7] The strong suppression of the higher multipoles is also due to angular momentum coupling in the intrinsic frame.

C. Total form factors. Comparison with experiment

Results for elastic and inelastic transverse form factors of ^{166}Er, ^{181}Ta, ^{165}Ho, and ^{159}Tb are shown in Figs. 11–16. Corrections for nucleon finite size[15] and center of mass effects have been included (see Appendix A). The usual correction[16] corresponding to spherical oscillator wave functions has been used for the center of mass effect. It has been pointed out[17] that when projecting states of good angular momentum from an axially symmetric HF wave function one picks up nonspherical components of the center of mass wave function and therefore one may get additional unphysical contributions to the form factors. A schematic calculation shows that under the factorization assumptions in Ref. 17 these additional corrections are to leading order proportional to $(bq/2)^2 \cdot \delta/A$, and can therefore be neglected in our case ($\delta \sim 0.3$, $A > 160$).

In Fig. 11 we show the predictions for the total inelastic transverse form factors of ^{166}Er. As already pointed out, such an even-even rotator provides a direct measure of the core contribution to the nuclear current distribution. Each transition only depends on a single multipole. However, the predicted form factors are small and may be difficult to isolate experimentally. An experiment[12] to measure these effects is currently in progress at Bates.

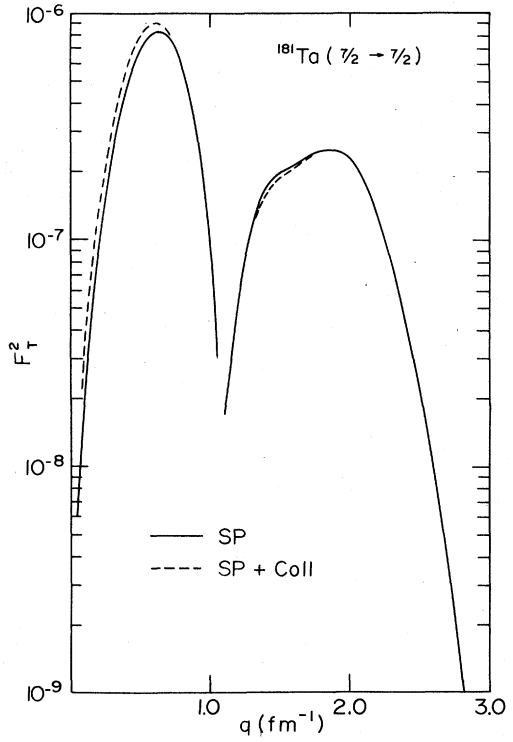

FIG. 10. Comparison of single particle (s.p.) and total (s.p. + col) transverse form factor squared for elastic scattering on ^{181}Ta corresponding to no pairing. Similar results are obtained in the case of pairing (see Figs. 7 and 12).

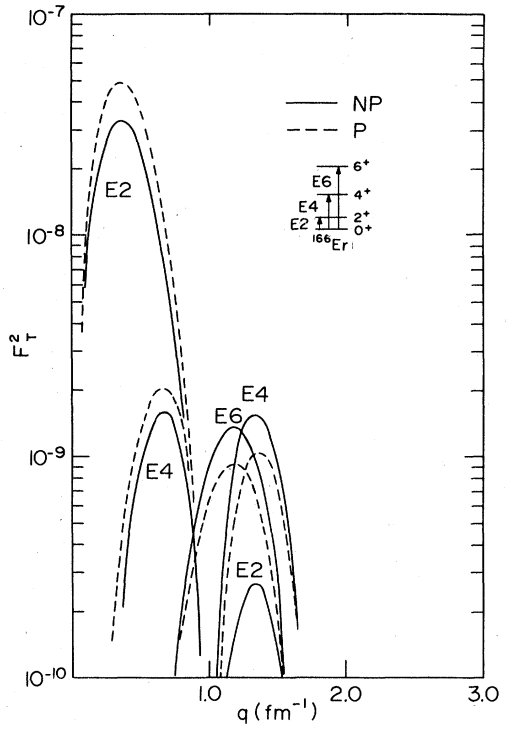

FIG. 11. Total transverse form factors for inelastic scattering on ^{166}Er ($0^+ \rightarrow 2^+$, 4^+, 6^+). Results corresponding to pairing (P) and no pairing (NP) are represented by dashed and full lines, respectively. These results contain corrections for nucleon finite size and center of mass effects (see text).

In Figs. 12–14 the results on ^{181}Ta are compared with the experimental data of Rad *et al.*[1] Since these calculations are based on the PWBA, in order to account for distortions the data have been plotted as a function of the momentum transfer q_{eff}.[5] These few data points over a very limited region of momentum transfer do not allow for any quantitative conclusions to be drawn at this time. What may be concluded, however, is that such measurements of transverse form factors are very sensitive to the exact nature of the wave function of the odd nucleon and, in turn, to the exact nature of the deformed core.

The effect of the strong coupling of the wave function for the odd proton to the deformed nuclear potential is clearly observed experimentally. Although the predictions are close, the data appear to require that the $M7$ multipole is shifted to peak at higher momentum transfers than the calculations. More extensive and accurate data is clearly required in order to correctly limit the shape and extent of this multipole.

In Figs. 15 and 16 we show the results for ^{165}Ho and ^{159}Tb. The predictions for ^{165}Ho, which also has $I_i = K = \frac{7}{2}$, are quite different when compared with those for ^{181}Ta. In the case of elastic scattering (as well as in the $\frac{7}{2} \rightarrow \frac{9}{2}$ transition) this difference comes entirely from the intrinsic multipoles $F_K^{M\lambda}(q)$ and $F_{2K}^{M\lambda}(q)$. The odd proton HF states are approximately given by the Nilsson orbitals [404↓] and [523↑] in the cases of ^{181}Ta and ^{165}Ho, respectively. The difference in the strengths, shapes, and locations of the peaks in Figs. 12 and 15 are almost entirely due to the different properties of those orbitals. For the $\frac{7}{2} \rightarrow \frac{11}{2}$ transition, the effect of the $M9$ multipole may be seen at high momentum transfer ($q \gtrsim 1.5$), whereas in ^{181}Ta it is dominated by the $M7$.

^{159}Tb with $I_i = K = \frac{3}{2}$, has contributions from $M1$ and $M3$ multipoles in elastic scattering. Single particle effects are again most important, with the $M1$ multipole being dominant at low momentum transfer. The subsidiary maxima at high momentum transfer arise from secondary peaks in the contributions from $M1$ and $M3$. For the $\frac{3}{2} \rightarrow \frac{7}{2}$ transition, where the $M1$ no longer contributes, the high momentum transfer region is mainly due to $E4$ and $M5$ single particle contributions.

In Table I we give a comparison of the results at $q\hbar c = 0.2$ MeV for single particle and rotational

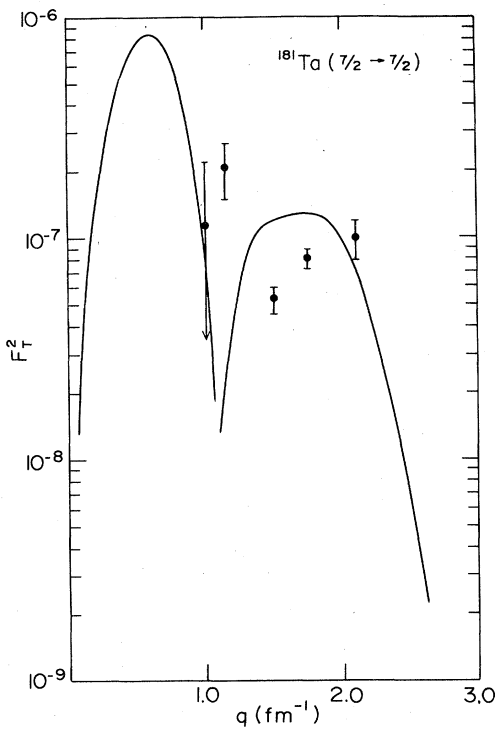

FIG. 12. Total transverse form factor for elastic scattering on ^{181}Ta (see caption to Fig. 11). The points with error bars represent experimental data (Ref. 1).

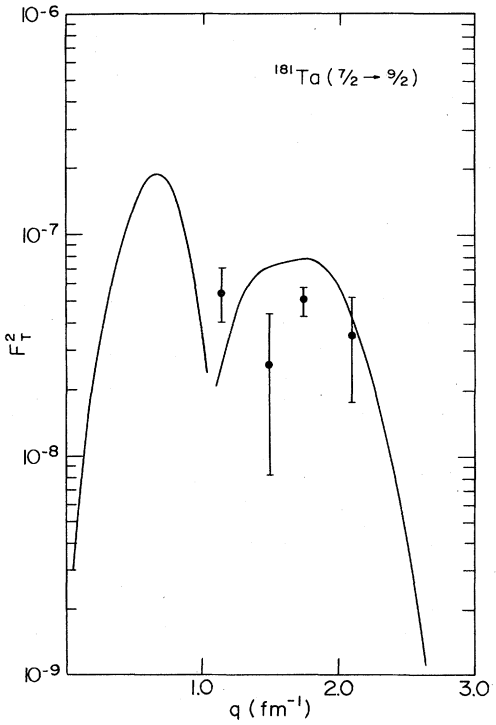

FIG. 13. Same as Fig. 12 for inelastic scattering $\frac{7}{2} \rightarrow \frac{9}{2}$ in the ground-state band.

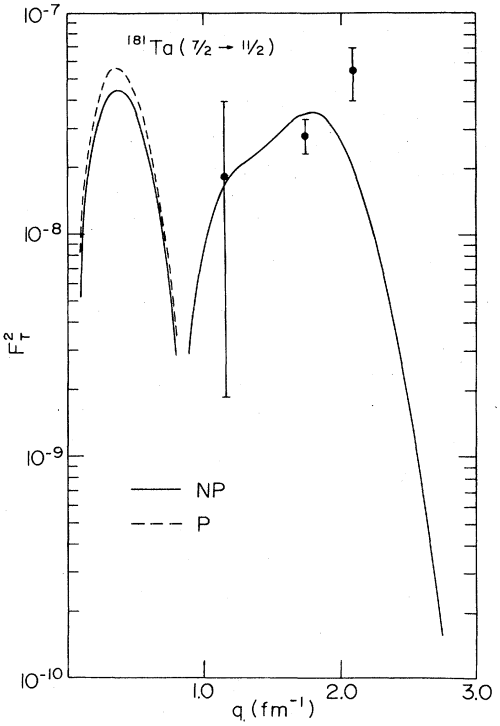

FIG. 14. Same as Fig. 12 for the transition $\frac{7}{2} \rightarrow \frac{11}{2}$ in the ground-state band.

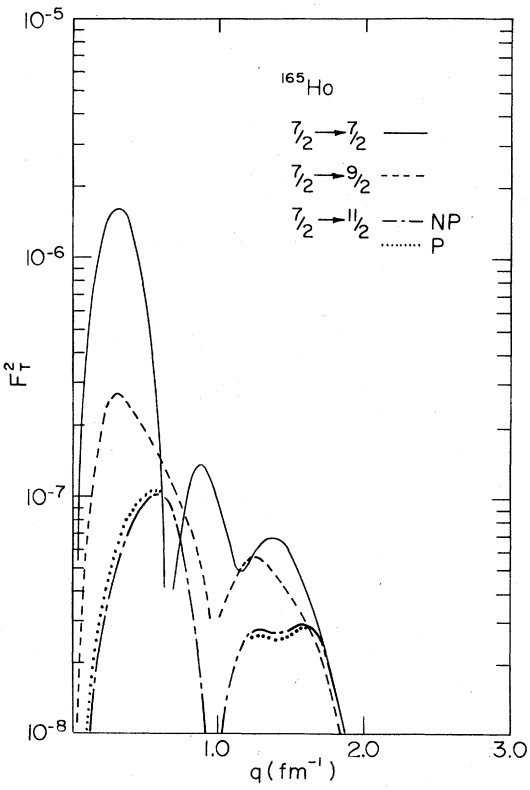

FIG. 15. Total transverse form factor for the three lowest ground-state rotational band transitions in ^{165}Ho. See caption to Fig. 11.

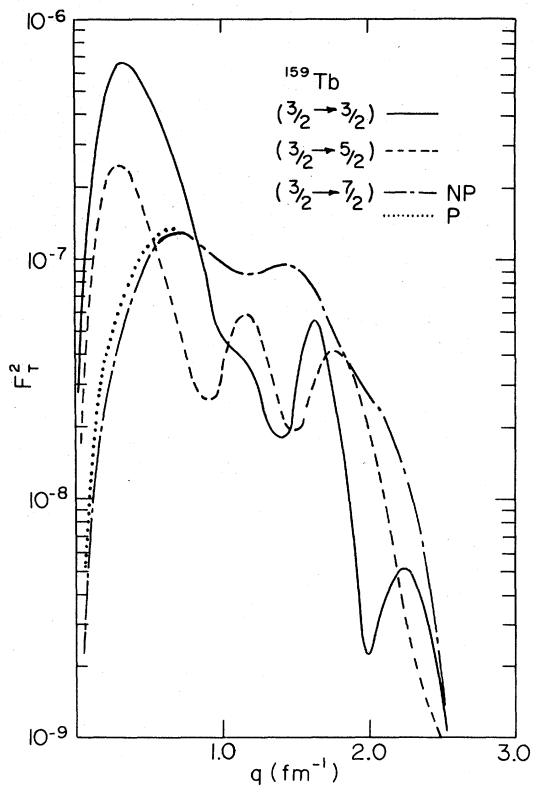

FIG. 16. Total transverse form factor for the three lowest ground-state rotational band transitions in ^{159}Tb. See caption to Fig. 11.

form factors (F_K^{M1}, F_R^{M1}, and F_R^{E2}) with those derived from experimental g_K, g_R ratios[7,8] and quadrupole moments [F_K^{M1}(exp), F_R^{M1}(exp), F_R^{E2}(exp)]; see Eqs. (2.7)–(2.10). The moments of inertia have been extracted from experimental energies of first excited states.[18] The agreement between F_R^{M1} and F_R^{M1}(exp) is quite good, as was to be expected from the agreement of theoretical and experimental g_R values[7] and can be considered as an additional check of our form factor calculations. Similarly, the discrepancies between theoretical and "experimental" F_K^{M1} values is analogous to those of g_K values[7] and are removed by using the effective g_s values given in Table IV of Ref. 7. As discussed in the previous subsection the use of g_s^{eff} does not modify in a significant way the single particle form factors at higher q values and has not been enforced here. As for F_R^{E2} it can be seen that in all cases it is approximately twice as large as the "experimental" one. It could be argued that this is due to the fact that the PHF moment of inertia is smaller than the experimental one.[6,19]. However, one must keep in mind that the continuity equation is not even satisfied within the model.[4] To remove this discrepancy, the continuity equation may be used beforehand to relate a part of $F_R^{E\lambda}$ to $F^{C\lambda}/\vartheta$ [see Eq. (B1) in Appendix B]. This has the disadvantage that different parts of the current are treated on a different footing and, although it leads to the correct result in the low q limit there is no guarantee that the results at higher q will be more reliable. A calculation for the simple model described at the end of Appendix A shows that the results at the first peak of the $E2$ are similar when using Eqs. (A7) and (B1). The value of the moment of inertia for the model was chosen so that at $q\hbar c = 0.2$ MeV the result from (A7) was twice that from (B1) as in the realistic cases of Table I.

IV. CONCLUSIONS AND FINAL REMARKS

We have investigated the predictions of the PHF approach on transverse form factors of rotational nuclei (^{166}Er, ^{181}Ta, ^{165}Ho, ^{159}Tb) for elastic and inelastic electron scattering within the ground-state rotational band.

From the results in Sec. III it can be concluded that the dominant contribution to transverse form

TABLE I. Comparison of theoretical and "experimental" intrinsic form factors (as defined in text) at $q\hbar c = 0.2$ MeV. Theoretical F_K^{M1} ($q = 10^{-3}$ fm^{-1}) values corresponding to $g_s^{\text{eff}}/g_s^{\text{free}} = 0.48$, 0.69, and 0.67 for Ta, Ho, and Tb, respectively (Ref. 7) are within parentheses. The lower and upper entries in columns two and six correspond to results with and without pairing, respectively. The experimental values have been deduced from Eqs. (2.7)–(2.12) as explained in the text. The experimental intrinsic quadrupole moments used are those quoted in Refs. 10, 5, 21, and 22 for Er, Ta, Ho, and Tb, respectively.

	F_R^{M1}	F_R^{M1} (exp)	F_K^{M1}	F_K^{M1}(exp)	F_R^{E2}	F_R^{E2}(exp)
$^{166}_{68}$Er	-4.64×10^{-7}	$-4.22(\pm0.38)\times10^{-7}$			1.37×10^{-7}	$7.06(\pm0.06)\times10^{-8}$
	-5.26×10^{-7}				1.71×10^{-7}	
$^{181}_{73}$Ta	-4.17×10^{-7}	$-3.81(\pm0.24)\times10^{-7}$	-1.54×10^{-6}	$-3.21(\pm0.04)\times10^{-6}$	1.40×10^{-7}	$7.17(\pm0.13)\times10^{-8}$
	-4.33×10^{-7}		(-3.21×10^{-6})		1.60×10^{-7}	
$^{165}_{67}$Ho	-4.58×10^{-7}	$-5.71(\pm0.52)\times10^{-7}$	-7.17×10^{-6}	$-6.04(\pm0.14)\times10^{-6}$	1.32×10^{-7}	$5.75(\pm0.05)\times10^{-8}$
	-5.23×10^{-7}		(-6.18×10^{-6})		1.65×10^{-7}	
$^{159}_{65}$Tb	-5.14×10^{-7}	$-5.62(\pm0.54)\times10^{-7}$	-4.80×10^{-6}	$-3.67(\pm0.10)\times10^{-6}$	1.37×10^{-7}	$5.80(\pm0.48)\times10^{-8}$
	-5.21×10^{-7}		(-3.68×10^{-6})		1.65×10^{-7}	

factors of odd-A nuclei comes from the odd nucleon, except for inelastic scattering at low momentum transfers where the collective transverse electric form factor dominates the picture for $\Delta I = 2$. In addition, cross sections at 180° for inelastic scattering on doubly even nuclei can be expected to be at least one order of magnitude lower than those for elastic scattering in odd-A nuclei. Little can be said about the validity of the different approximations until more extensive and accurate experimental data are available.

A comparison of the results on ^{181}Ta, ^{165}Ho, and ^{159}Tb illustrates the kind of changes to be expected in the transverse form factors for different odd-A rotators. These changes are for the most part due to the different orbitals occupied by the odd nucleon and/or the different K value for the ground-state rotational band in these cases.

A serious shortcoming of the PHF approach has been found (see Table I) by a comparison at very low q of rotational transverse electric form factors in this approach with those deduced from the continuity equation. We observe a factor of 2 between the predicted and deduced values of F_R^{E2} at low q.

As pointed out in Ref. 4 a better approximation to the form factors would be provided by solving the variation after projection equations of Villars and Schmeing-Rogerson.[6] Implementing the self consistency required by those equations may be difficult, but a good approximation to the transverse form factors of rotational nuclei can be obtained by a consistent first order expansion in $I_\pm$.[3] In this approximation the calculations of $F_R^{M\lambda}$ and $F_R^{E\lambda}$ are analogous[3] to those of gyromagnetic ratios in the cranking model by Prior *et al.*[20] These calculations require simple modifications in our present computer codes and will be done in the near future.

For odd-A nuclei, the limitations imposed by the pair filling approximation used to solve the HF equations may be more important than those due to projection after variation. As discussed in Sec. III B the use of effective g_s values[7,8] has very little effect on the results for single particle form factors. However, the q dependence of spin polarization effects may not be well simulated by modifying the g_s (or g_l) value. Experimental data on elastic scattering at low q ($0.3 \lesssim q \lesssim 0.7$) would be of great interest in order to clarify this question.

ACKNOWLEDGMENTS

We would like to express our appreciation to many of our colleagues both at the Center for Theoretical Physics and the Bates Linac for encouragement and helpful discussions related to this work. Thanks are due to Professor F. Villars for his critical reading of the manuscript and many comments. It is a pleasure to acknowledge many discussions on rotators, invaluable suggestions, critical comments, and the support of Professor W. Bertozzi. F. N. Rad provided the experimental data prior to pulication. One of us (E.M.G.) is indebted to Professor A. Bohr, Professor B. Mottelson, and Professor R. Peierls for many interesting suggestions, to the Niels Bohr Institute for its kind hospitality, and to the National Science Foundation for partial financial support. This work was supported in part through funds for the Bates Accelerator Laboratory provided by the U. S. Department of Energy (DOE) under Contract No. EY-76-C-02-3069.

APPENDIX A

In the HF codes for axially symmetric deformed nuclei[10,11] the single particle states are characterized by the quantum numbers π (parity) and m (angular momentum component along the symmetry axis J_z), and the $(Z/2)$ $(N/2)$ pairs of protons (neutrons) fill conjugate orbitals $(A, \bar{A})$:

$$\phi_{A\,m}^{\pi} = \phi_A^+(r,z)e^{i(m-1/2)\varphi}\chi_{1/2} + \phi_A^-(r,z)e^{i(m+1/2)\varphi}\chi_{-1/2},$$

$$\phi_{\bar{A}\,m}^{\pi} = -\phi_A^-(r,z)e^{i(-m-1/2)\varphi}\chi_{1/2} + \phi_A^+(r,z)e^{i(-m+1/2)\varphi}\chi_{-1/2}, \quad m>0.$$

The spin up and down functions (ϕ_A^+, ϕ_A^-) in the r,z plane—given as linear combinations of products of Laguerre and Hermite polynomials[11]—are determined by iterating to self-consistency and then used to compute the form factors (2.12) to (2.16) as described below.

For odd-A nuclei the orbital of the odd nucleon is selected in the last iteration according to the experimental π and K numbers, among the last occupied orbitals. Denoting its spin up and down amplitudes by ϕ_K^+ and ϕ_K^- the intrinsic form factors [(2.12), (2.13), (2.15)] are given by

$$F_K^{M\lambda}(q) = C(q) i^{\lambda+1} \iint \Big\{ e \Big[\frac{2\lambda+1}{\lambda(\lambda+1)}\Big]^{1/2} j_\lambda P_\lambda^1 \Big[\frac{2K-1}{2r}(\phi_K^+)^2 + \frac{2K+1}{2r}(\phi_K^-)^2\Big] + q\mu \Big[\frac{\lambda(\lambda+1)}{2\lambda+1}\Big]^{1/2} \{(j_{\lambda+1}P_{\lambda+1}^0 + j_{\lambda-1}P_{\lambda-1}^0)\tfrac{1}{2}[(\phi_K^+)^2 - (\phi_K^-)^2] + [j_{\lambda+1}P_{\lambda+1}^1/(\lambda+1) - j_{\lambda-1}P_{\lambda-1}^1/\lambda]\phi_K^+\phi_K^-\}\Big\}, \tag{A1}$$

$$F_{2K}^{M\lambda}(q) = C(q) i^{\lambda+1} \Big[\frac{(\lambda-2K)!}{(\lambda+2K)!}\Big]^{1/2} \iint \Big\{ e \Big[\frac{2\lambda+1}{\lambda(\lambda+1)}\Big]^{1/2} j_\lambda P_\lambda^{2K} \Big(\frac{2K-1}{r}\phi_K^+\nabla_\theta\phi_K^- - \frac{2K+1}{r}\phi_K^-\nabla_\theta\phi_K^+\Big) + q\mu \Big[\frac{\lambda(\lambda+1)}{2\lambda+1}\Big]^{1/2} \Big[\Big(j_{\lambda+1}P_{\lambda+1}^{2K}\frac{\lambda-2K+1}{\lambda+1} + j_{\lambda-1}P_{\lambda-1}^{2K}\frac{\lambda+2K}{\lambda}\Big)\phi_K^+\phi_K^- + \Big(j_{\lambda+1}P_{\lambda+1}^{2K-1}\frac{(\lambda-2K+1)(\lambda-2K+2)}{2(\lambda+1)} - j_{\lambda-1}P_{\lambda-1}^{2K-1}\frac{(\lambda+2K-1)(\lambda+2K)}{2\lambda}\Big)(\phi_K^+)^2 + \Big(j_{\lambda+1}P_{\lambda+1}^{2K+1}\frac{1}{2(\lambda+1)} - j_{\lambda-1}P_{\lambda-1}^{2K+1}\frac{1}{2\lambda}\Big)(\phi_K^-)^2\Big]\Big\}, \tag{A2}$$

$$F_{2K}^{E\lambda}(q) = C(q) i^{\lambda} \Big[\frac{(\lambda-2K)!(2\lambda+1)}{(\lambda+2K)!\lambda(\lambda+1)}\Big]^{1/2} \iint \Big\{ \mu q j_\lambda [2K P_\lambda^{2K}\phi_K^+\phi_K^- + \tfrac{1}{2}(\lambda+2K)(\lambda-2K+1)P_\lambda^{2K-1}(\phi_K^+)^2 - \tfrac{1}{2}P_\lambda^{2K+1}(\phi_K^-)^2] + \frac{e}{qR}\Big[j_\lambda P_\lambda^{2K}\lambda(\lambda+1)2\phi_K^+\nabla_R\phi_K^- + \frac{q}{2\lambda+1}[(\lambda+1)j_{\lambda-1} - \lambda j_{\lambda+1}] \times \Big(P_\lambda^{2K}\frac{2K(2K+1)}{\sin^2\theta}\phi_K^+\phi_K^- + [(\lambda+2K)(\lambda-2K+1)P_\lambda^{2K-1} - P_\lambda^{2K+1}]\phi_K^+\nabla_\theta\phi_K^-\Big)\Big]\Big\}, \tag{A3}$$

with $\mu = 2.79\ (-1.91)$, $e = 1\ (0)$ for odd $Z(N)$. The following abbreviations are used:

$$\iint = \int R^2 dR \int_0^1 d\cos\theta, \tag{A4}$$

$$C(q) = \frac{4\pi}{Z}\frac{\hbar}{Mc} f(q), \quad f(q) = \exp\Big[\Big(-\frac{(0.8)^2}{6} + \frac{b^2}{4A}\Big)q^2\Big], \tag{A5}$$

where $f(q)$ is the product of the nucleon and (inverse) center of mass form factors. Note that $r = R\sin\theta$, $z = R\cos\theta$, $j_l \equiv j_l(qR)$, and $P_l^m \equiv P_l^m(\cos\theta)$. The collective form factors (2.14) and (2.16) are given by

$$F_R^{M\lambda}(q) = \frac{C(q) i^{\lambda+1}(-\sqrt{2})}{(2\lambda+1)^{1/2}\langle J_\perp^2\rangle} \iint \sum_{\alpha=p,n} \Big\{ e_\alpha \frac{2\lambda+1}{\lambda(\lambda+1)} j_\lambda \frac{1}{r}\{P_\lambda^1 \mathfrak{M}\mathfrak{C}_1^\alpha + \tfrac{1}{2}[\lambda(\lambda+1)P_\lambda^0 - P_\lambda^2]\mathfrak{M}\mathfrak{C}_2^\alpha\} + \frac{q\mu_\alpha}{2}\Big[\Big(\frac{\lambda}{\lambda+1}j_{\lambda+1}P_{\lambda+1}^1 + \frac{\lambda+1}{\lambda}j_{\lambda-1}P_{\lambda-1}^1\Big)\mathfrak{M}\mathfrak{M}\mathfrak{T}_1^\alpha + [-\lambda j_{\lambda+1}P_{\lambda+1}^0 + (\lambda+1)j_{\lambda-1}P_{\lambda-1}^0]\mathfrak{M}\mathfrak{M}\mathfrak{T}_2^\alpha + \Big(-\frac{1}{\lambda+1}j_{\lambda+1}P_{\lambda+1}^2 + \frac{1}{\lambda}j_{\lambda-1}P_{\lambda-1}^2\Big)\mathfrak{M}\mathfrak{M}\mathfrak{T}_3^\alpha\Big]\Big\}, \tag{A6}$$

$$F_R^{E\lambda}(q) = \frac{C(q) i^{\lambda}}{[(2\lambda+1)\lambda(\lambda+1)]^{1/2}\langle J_\perp^2\rangle} \iint \sum_{\alpha=p,n} \Big\{ \frac{q\mu_\alpha}{2}\frac{2\lambda+1}{\lambda(\lambda+1)} j_\lambda [P_\lambda^1 \mathcal{E}\mathfrak{M}\mathfrak{T}_1^\alpha - \lambda(\lambda+1)P_\lambda^0 \mathcal{E}\mathfrak{M}\mathfrak{T}_2^\alpha + P_\lambda^2 \mathcal{E}\mathfrak{M}\mathfrak{T}_3^\alpha] + e_\alpha\Big[\Big(\frac{\lambda}{\lambda+1}j_{\lambda+1}P_{\lambda+1}^1 + \frac{\lambda+1}{\lambda}j_{\lambda-1}P_{\lambda-1}^1\Big)\frac{1}{r}\mathcal{E}\mathfrak{C}_1^\alpha - P_\lambda^1\frac{(j_{\lambda+1}+j_{\lambda-1})}{\sin\theta}\mathcal{E}\mathfrak{C}_2^\alpha - P_\lambda^1\frac{1}{r\sin\theta}\Big(-\frac{1}{\lambda+1}j_{\lambda+1} + \frac{1}{\lambda}j_{\lambda-1}\Big)\mathcal{E}\mathfrak{C}_3^\alpha\Big]\Big\}. \tag{A7}$$

The densities $\mathfrak{me}_i^{\alpha}$, $\mathfrak{mm}_i^{\alpha}$, $\mathcal{E}\mathfrak{e}_i^{\alpha}$, $\mathcal{E}\mathfrak{m}_i^{\alpha}$ in Eqs. (A6) and (A7) are given below:

$$\mathfrak{mm}_1^{p(n)} = -\sum I_{AB}(\phi_B^+\phi_A^+ - \phi_B^-\phi_A^-) + \tfrac{1}{2}\sum{}' I_{A\bar{B}}(\phi_A^+\phi_B^- + \phi_A^-\phi_B^+) + \delta_{Z(N),\mathrm{odd}}\frac{z}{r}\left[(K-\tfrac{1}{2})^2(\phi_K^+)^2 - (K+\tfrac{1}{2})^2(\phi_K^-)^2\right], \tag{A8}$$

$$\mathfrak{mm}_2^{p(n)} = -\sum I_{AB}\phi_B^+\phi_A^- - \tfrac{1}{2}\sum{}' I_{A\bar{B}}\phi_A^+\phi_B^+ + \delta_{Z(N),\mathrm{odd}}\tfrac{1}{2}\left[\phi_K^+(\tilde{\nabla}_\theta + 2Kz/r)\phi_K^- - (\phi_K^+)^2 - (\phi_K^-)^2\right], \tag{A9}$$

$$\mathfrak{mm}_3^{p(n)} = \sum I_{AB}\phi_B^-\phi_A^+ - \tfrac{1}{2}\sum{}' I_{A\bar{B}}\phi_A^-\phi_B^- + \delta_{Z(N),\mathrm{odd}}\tfrac{1}{2}\left[\phi_K^+(\tilde{\nabla}_\theta - 2Kz/r)\phi_K^-\right], \tag{A10}$$

with $\phi_a\tilde{\nabla}_\theta\phi_b \equiv \phi_a\nabla_\theta\phi_b - \phi_b\nabla_\theta\phi_a$,

$$\mathfrak{me}_1^{p(n)} = -\sum I_{AB}(\phi_B^+\nabla_\theta\phi_A^+ + \phi_B^-\nabla_\theta\phi_A^-) - \tfrac{1}{2}\sum{}' I_{A\bar{B}}(\phi_B^-\nabla_\theta\phi_A^+ + \phi_A^-\nabla_\theta\phi_B^+) + \delta_{Z(N),\mathrm{odd}} \times\left[\phi_K^+\nabla_\theta\phi_K^- - |\nabla_\theta\phi_K^+|^2 - |\nabla_\theta\phi_K^-|^2\right], \tag{A11}$$

$$\mathfrak{me}_2^{p(n)} = \sum I_{AB}\left[(m-\tfrac{1}{2})\phi_B^+\phi_A^+ + (m+\tfrac{1}{2})\phi_B^-\phi_A^-\right] + \delta_{Z(N),\mathrm{odd}}\left\{(K+\tfrac{1}{2})\left|\phi_K^+\phi_K^- - (z/r)\left[(K-\tfrac{1}{2})^2(\phi_K^+)^2 + (K+\tfrac{1}{2})^2(\phi_K^-)^2\right]\right\}, \tag{A12}$$

$$\mathcal{E}\mathfrak{m}_1^{p(n)} = -\sum I_{AB}(\phi_B^+\phi_A^+ - \phi_B^-\phi_A^-) + \tfrac{1}{2}\sum{}' I_{A\bar{B}}(\phi_A^+\phi_B^- + \phi_A^-\phi_B^+) + \delta_{Z(N),\mathrm{odd}}\left\{K\frac{z}{r}\left[(\phi_K^+)^2 - (\phi_K^-)^2 - 2\frac{z}{r}\phi_K^+\phi_K^-\right]\right\}, \tag{A13}$$

$$\mathcal{E}\mathfrak{m}_2^{p(n)} = -\sum I_{AB}\phi_B^+\phi_A^- - \tfrac{1}{2}\sum{}' I_{A\bar{B}}\phi_A^+\phi_B^+ + \delta_{Z(N),\mathrm{odd}}\tfrac{1}{2}\left[\phi_K^+\tilde{\nabla}_\theta\phi_K^- - \tfrac{1}{2}(\phi_K^+)^2 - \tfrac{1}{2}(\phi_K^-)^2\right], \tag{A14}$$

$$\mathcal{E}\mathfrak{m}_3^{p(n)} = \sum I_{AB}\phi_B^-\phi_A^+ - \tfrac{1}{2}\sum{}' I_{A\bar{B}}\phi_A^-\phi_B^- + \delta_{Z(N),\mathrm{odd}}\tfrac{1}{2}\left[\phi_K^+\tilde{\nabla}_\theta\phi_K^- - \tfrac{1}{2}(\phi_K^+)^2 - \tfrac{1}{2}(\phi_K^-)^2\right], \tag{A15}$$

$$\mathcal{E}\mathfrak{e}_1^{p(n)} = \sum I_{AB}(\phi_B^+\nabla_\theta\phi_A^+ + \phi_B^-\nabla_\theta\phi_A^-) - \tfrac{1}{2}\sum{}' I_{A\bar{B}}(\phi_A^+\nabla_\theta\phi_B^- - \phi_A^-\nabla_\theta\phi_B^+) + \delta_{Z(N),\mathrm{odd}}\left[|\nabla_\theta\phi_K^+|^2 + |\nabla_\theta\phi_K^-|^2 - \phi_K^+\nabla_\theta\phi_K^-\right], \tag{A16}$$

$$\mathcal{E}\mathfrak{e}_2^{p(n)} = \sum I_{AB}(\phi_B^+\nabla_r\phi_A^+ + \phi_B^-\nabla_r\phi_A^-) - \tfrac{1}{2}\sum{}' I_{A\bar{B}}(\phi_A^+\nabla_r\phi_B^- - \phi_A^-\nabla_r\phi_B^+) + \delta_{Z(N),\mathrm{odd}}\left[(\nabla_r\phi_K^+)(\nabla_\theta\phi_K^+) + (\nabla_r\phi_K^-)(\nabla_\theta\phi_K^-) - \phi_K^+\nabla_r\phi_K^-\right], \tag{A17}$$

$$\mathcal{E}\mathfrak{e}_3^{p(n)} = -\sum I_{AB}\left[(m-\tfrac{1}{2})\phi_B^+\phi_A^+ + (m+\tfrac{1}{2})\phi_B^-\phi_A^-\right] - \tfrac{1}{2}\sum{}' I_{A\bar{B}}\phi_A^+\phi_B^- + \delta_{Z(N),\mathrm{odd}}\left\{\frac{z}{r}\left[(K-\tfrac{1}{2})^2(\phi_K^+)^2 + (K+\tfrac{1}{2})^2(\phi_K^-)^2 - (K+\tfrac{1}{2})\phi_K^+\phi_K^-\right]\right\}. \tag{A18}$$

In Eqs. (A8)–(A18) the following abreviated notation has been used:

$$\sum I_{AB}F_{AB}(r,z) \equiv \sum_{A_{m>0}}\sum_{B_{m+1}}\theta_{AB}\langle B_{m+1}|j_+|A_m\rangle \times F_{AB}(r,z), \tag{A19}$$

$$\sum{}' I_{A\bar{B}}F_{AB}(r,z) \equiv \sum_{A_{1/2}}\sum_{B_{1/2}}\theta_{AB}\langle A_{1/2}|j_+|\bar{B}_{1/2}\rangle \times F_{AB}(r,z), \tag{A20}$$

with θ_{AB} as given in Eq. (2.19) and $\langle B|j_+|A\rangle$, $\langle A|j_+|\bar{B}\rangle$ (as well as $\langle J_\perp^2\rangle$) as calculated in Ref. 7. The sums on A, B run over proton (neutron) states of equal parity, and in the case of odd Z (N), A and B must be different from the state of the odd proton (neutron).

Equations (A8)–(A20) correspond to Eq. (2.17). The use of Eq. (2.17)′) leads to more involved expressions for the densities that can be derived from Eqs. (A8)–(A18) by replacing θ_{AB} by $-2\theta'_{AB}$ [see Eq. (2.18)] and the term $\delta_{Z(N),\mathrm{odd}}\cdot f(\phi_K^+,\phi_K^-)$ by

$$\sum_{A_{m>0}}(n_A + (\tfrac{1}{2} - n_A)\delta_{A,K})2f(\phi_A^+,\phi_A^-)$$

(see also the Appendix to Ref. 7).

The numerical calculations were performed according to the following scheme: (1) The densities (A8)–(A18) as well as the single particle densities in Eqs. (A1)–(A3) were calculated at the mesh points. (2) For every density $\rho_i(r,z)$ a polynomial $P_i(r^2,z^2)$ of degree N_0 in both r^2 and z^2 is found[11] that satisfies

$$\rho_i(r,z)=e^{-\beta_z z^2}e^{-\beta_\perp r^2}f_i(r,z)P_i(r^2,z^2)\,, \qquad \text{(A21)}$$

where $f_i(r,z)=r^{-n_i}\cdot z^{-n'_i}$ with $n_i=0$ ($n'_i=0$) if $\rho_i(r,z)$ is an even function of $r(z)$, and $n_i=1$ ($n'_i=1$) if $\rho_i(r,z)$ is an odd function of $r(z)$. (3) The numerical integrations on θ and R (in that order) were performed using the densities (A21). (4) The resulting form factors $F_K^{M\lambda}(q)$, $F_{2K}^{M\lambda}(q)$, $F_R^{M\lambda}(q)$, $F_R^{E\lambda}(q)$, and $F_{2K}^{E\lambda}(q)$ were combined according to Eq. (2.4) [(2.5) or (2.6)] for a given transition. Multipolarities $\lambda \geq 10$ have been neglected.

The computer codes were tested with a model of 12 protons and 12 neutrons (6 deformed orbitals in all) for which the form factors were calculated analytically.

APPENDIX B

An alternative expression for $T_\mu^{E\lambda}$ (see p. 51 of Ref. 9) can be used to relate part of the transverse electric form factor to the experimental energy difference. This leads to the following alternative expression for $F_R^{E\lambda}(q)$:

$$F_R^{E\lambda}(q)=-\left(\frac{\lambda+1}{\lambda}\right)^{1/2}\frac{F^{c\lambda}(q)}{\hbar c q(2\mathcal{I}/\hbar^2)}+\frac{C(q)i^\lambda}{[(2\lambda+1)\lambda(\lambda+1)]^{1/2}\langle J_\perp^2\rangle}$$

$$\times\iint\sum_{\alpha=p,n}\left\{e_\alpha\left[\tfrac{1}{2}qj_\lambda P_\lambda^1\mathcal{E}\mathfrak{C}_4^\alpha+\frac{(2\lambda+1)}{\lambda}j_{\lambda+1}\left(\frac{\lambda}{\lambda+1}P_{\lambda+1}^1\frac{1}{r}\mathcal{E}\mathfrak{C}_1^\alpha-\frac{P_\lambda^1}{\sin\theta}\mathcal{E}\mathfrak{C}_2^\alpha+\frac{1}{\lambda+1}\frac{P_\lambda^1}{r\sin\theta}\mathcal{E}\mathfrak{C}_3^\alpha\right)\right]\right.$$

$$\left.+\frac{q\mu_\alpha}{2}\frac{2\lambda+1}{\lambda(\lambda+1)}j_\lambda[P_\lambda^1\mathcal{E}\mathfrak{M}_1^\alpha-\lambda(\lambda+1)P_\lambda^0\mathcal{E}\mathfrak{M}_2^\alpha+P_\lambda^2\mathcal{E}\mathfrak{M}_3^\alpha]\right\}\,, \qquad \text{(B1)}$$

where $\mathcal{I}$ is the experimental moment of inertia and

$$F^{c\lambda}(q)=\frac{4\pi}{Z}f(q)i^\lambda(2\lambda+1)^{1/2}\iint j_\lambda P_\lambda^0\rho_p\,. \qquad \text{(B2)}$$

ρ_p is the proton density

$$\rho_p(r,z)=2\sum_{A_m>0}n_A(|\phi_A^+|^2+|\phi_A^-|^2)\,. \qquad \text{(B3)}$$

The densities $\mathcal{E}\mathfrak{C}_i^\alpha$, $\mathcal{E}\mathfrak{M}_i^\alpha(i=1,2,3)$ are as defined in Appendix A, and $\mathcal{E}\mathfrak{C}_4^\alpha$ is given by

$$\mathcal{E}\mathfrak{C}_4^\alpha=-\sum I_{AB}(\phi_A^+\phi_B^+ +\phi_A^-\phi_B^-)\,. \qquad \text{(B4)}$$

---

[1] F. N. Rad, private communication and unpublished.

[2] See, for instance, T. W. Donnelly and J. D. Walecka, Nucl. Phys. A201, 81 (1973).

[3] E. Moya de Guerra, Ann. Phys. (N.Y.) (to be published).

[4] E. Moya de Guerra and A. L. Dieperink, Phys. Rev. C 18, 1596 (1978); in *Proceedings of the June Workshop in Intermediate Energy Electromagnetic Interactions with Nuclei*, edited by A. M. Bernstein (MIT, Cambridge, 1977), p. 372. Note that in this first reference there is a mistake in the scale of Fig. 2 which should read one order of magnitude lower for comparison with Fig. 1.

[5] F. N. Rad *et al.*, Phys. Rev. Lett. 40, 368 (1978); W. Bertozzi, J. Phys. Soc. Jpn. Suppl. 44, 173 (1978); J. W. Negele, in Proceedings of the Conference on Modern Trends in Electron Scattering, Amsterdam, 1978 (unpublished), and references therein.

[6] R. E. Peierls and J. Yoccoz, Proc. Phys. Soc. London A70, 381 (1957); A70, 388 (1957); R. E. Peierls and D. J. Thouless, Nucl. Phys. 38, 154 (1962); F. Villars and N. Schmeing-Rogerson, Ann. Phys. (N.Y.) 63, 443 (1971).

[7] E. Moya de Guerra and S. Kowalski, Phys. Rev. C 20,

357 (1979).
[8]A. Bohr and B. Mottelson, *Nuclear Structure*, 5th ed. (Benjamin, New York, 1975), Vol. II.
[9]T. DeForest and J. D. Walecka, Adv. Phys. 15, 1 (1966).
[10]J. W. Negele and G. Rinker, Phys. Rev. C 15, 1499 (1977).
[11]D. Vautherin, Phys. Rev. C 7, 296 (1973).
[12]R. A. Lindgren, private communication.
[13]A. Zarringhalam and J. W. Negele, Nucl. Phys. A288, 417 (1977).
[14]G. Konopka, M. Gari, and J. G. Zabolitzky, Nucl. Phys. A290, 360 (1977); J. Dubach, J. H. Koch, and T. W. Donnelly, *ibid.* A271, 279 (1976).
[15]H. Überall, *Electron Scattering from Complex Nuclei*, parts A and B (Academic, New York, 1971).
[16]L. J. Tassie and E. C. Barber, Phys. Rev. 111, 940 (1958).
[17]D. J. Ernst, C. M. Shakin, and R. M. Thaler, Phys. Rev. C 8, 440 (1973).
[18]C. M. Lederer *et al.*, *Table of Isotopes*, 7th ed. (Wiley-Interscience, New York, 1978).
[19]D. Husain, Proc. Phys. Soc. London 91, 581 (1967).
[20]O. Prior, F. Boehm, and S. G. Nilsson, Nucl. Phys. A110, 257 (1968). For similar calculations of gyromagnetic ratios using HF wave functions see D. W. L. Sprung, S. G. Lie, and M. Vallieres, Nucl. Phys. (to be published).
[21]R. J. Powers *et al.*, Nucl. Phys. A262, 493 (1976).
[22]W. J. Childs, Phys. Rev. A 2, 316 (1970).